J|A|C|S ARTICLES

Published on Web 10/28/2010

Highly Efficient Gene Silencing Activity of siRNA Embedded in a Nanostructured Gyroid Cubic Lipid Matrix

Cecília Leal,* Nathan F. Bouxsein, Kai K. Ewert, and Cyrus R. Safinya*

Physics, Materials, and Molecular, Cellular & Developmental Biology Departments, University of California, Santa Barbara, California 93106, United States

Received July 6, 2010; E-mail: cecilial@mrl.ucsb.edu; safinya@mrl.ucsb.edu

Abstract: RNA interference (RNAi) is an evolutionarily conserved sequence-specific post-transcriptional gene silencing pathway with wide-ranging applications in functional genomics, therapeutics, and biotechnology. Cationic liposome−small interfering RNA (CL−siRNA) complexes have emerged as vectors of choice for delivery of siRNA, which mediates RNAi. However, siRNA delivery by CL−siRNA complexes is often inefficient and accompanied by lipid toxicity. We report the development of CL−siRNA complexes with a novel cubic phase nanostructure, which exhibit efficient silencing at low toxicity. The inverse bicontinuous gyroid cubic nanostructure was unequivocally established from synchrotron X-ray scattering data, while fluorescence microscopy revealed colocalization of lipid and siRNA in complexes. We attribute the efficient silencing to enhanced fusion of complex and endosomal membranes, facilitated by the cubic phase membrane's positive Gaussian modulus, which may enable spontaneous formation of transient pores. The findings underscore the importance of understanding membrane-mediated interactions between CL−siRNA complex nanostructure and cell components in developing CL-based gene silencing vectors.

Introduction

The landmark discovery (made more than two decades ago[1]) that cationic liposomes (CLs) are viable synthetic vectors for plasmid-DNA (i.e., gene) delivery is responsible for the current significant worldwide effort, including ongoing human gene therapy clinical trials,[2−4] to develop nonviral vectors competitive in transfection efficiency with engineered viral carriers.[5,6] The latter have on occasion led to severe immune reactions and insertional oncogenesis.[7−9]

More recently, the discovery that cytoplasmic delivery of exogenous small interfering RNA (siRNA) induces gene silencing[10,11] (as part of the RNA interference pathway[12−16]) has motivated major research efforts directed toward developing CL−siRNA complexes as efficient gene silencing vectors. Aside from functional genomics, applications of these vectors include therapeutics and biotechnology.[17−23]

The most common mechanism of cell entry for CL−nucleic acid complexes is via endocytosis.[24−28] Accordingly, entrapment of complexes in the endosome is a major barrier to cytoplasmic delivery of the nucleic acids because endosomal content eventually is subject to lysosomal degradation. Previous work with lamellar (L_α^C) CL−DNA complexes has revealed that complexes with low membrane charge density (σ_M, charge per

(1) Felgner, P. L.; Gadek, T. R.; Holm, M.; Roman, R.; Chan, H. W.; Wenz, M.; Northrop, J. P.; Ringold, G. M.; Danielsson, M. *Proc. Natl. Acad. Sci. U.S.A.* **1987**, *84*, 7413–7417.
(2) Edelstein, M. L.; Abedi, M. R.; Wixon, J.; Edelstein, R. M. *J. Gene Med.* **2004**, *6*, 597–602.
(3) See: http://www.wiley.co.uk/genetherapy/clinical.
(4) Edelstein, M. L.; Abedi, M. R.; Wixon, J. *J. Gene Med.* **2007**, *9*, 833–842.
(5) Huang, L.; Hung, M.-C.; Wagner, E. *Advances in Genetics, Vol. 53: Non-Viral Vectors for Gene Therapy*, 2nd ed., Part 1; Elsevier: San Diego, CA, 2005.
(6) Ewert, K.; Ahmad, A.; Evans, H. M.; Safinya, C. R. *Expert Opin. Biol. Ther.* **2005**, *5*, 33–53.
(7) Williams, D. A.; Baum, C. *Science* **2003**, *302*, 400–401.
(8) Thomas, C. E.; Ehrhardt, A.; Kay, M. A. *Nat. Rev. Genet.* **2003**, *4*, 346–358.
(9) Hacein-Bey-Abina, S.; et al. *J. Clin. Invest.* **2008**, *118*, 3132–3142.
(10) Elbashir, S. M.; Harborth, J.; Lendeckel, W.; Yalcin, A.; Weber, K.; Tuschl, T. *Nature* **2001**, *411*, 494–498.
(11) Caplen, N. J.; Parrish, S.; Imani, F.; Fire, A.; Morgan, R. A. *Proc. Natl. Acad. Sci. U.S.A.* **2001**, *98*, 9742–9747.
(12) Cogoni, C.; Macino, G. *Curr. Opin. Genet. Dev.* **2000**, *10*, 638–643.
(13) Fire, A.; Xu, S. Q.; Montgomery, M. K.; Kostas, S. A.; Driver, S. E.; Mello, C. C. *Nature* **1998**, *391*, 806–811.
(14) Hammond, S. M.; Caudy, A. A.; Hannon, G. J. *Nat. Rev. Genet.* **2001**, *2*, 110–119.
(15) Jorgensen, R.; Cluster, P. D.; English, J.; Que, Q.; Napoli, C. A. *Plant Mol. Biol.* **1996**, *31*, 957–973.
(16) Napoli, C. A.; Lemieux, C.; Jorgensen, R. *Plant Cell* **1990**, *2*, 279–289.
(17) Caplen, N. J. *Expert Opin. Biol. Ther.* **2003**, *3*, 575–586.
(18) Elbashir, S. M.; Harborth, J.; Weber, K.; Tuschl, T. *Methods* **2002**, *26*, 199–213.
(19) Hannon, G. J.; Rossi, J. J. *Nature* **2004**, *431*, 371–378.
(20) Karagiannis, T. C.; El-Osta, A. *Cancer Gene Ther.* **2005**, *12*, 787–795.
(21) Martinez, L. A.; Naguibneva, I.; Lehrmann, H.; Vervisch, A.; Tchenio, T.; Lozano, G.; Harel-Bellan, A. *Proc. Natl. Acad. Sci. U.S.A.* **2002**, *99*, 14849–14854.
(22) McManus, M. T.; Sharp, P. A. *Nat. Rev. Genet.* **2002**, *3*, 737–747.
(23) Sioud, M. *Trends Pharmacol. Sci.* **2004**, *25*, 22–28.
(24) Ahmad, A.; Evans, H. M.; Ewert, K.; George, C. X.; Samuel, C. E.; Safinya, C. R. *J. Gene Med.* **2005**, *7*, 739–748.
(25) Labat-Moleur, F.; Steffan, A. M.; Brisson, C.; Perron, H.; Feugeas, O.; Furstenberger, P.; Oberling, F.; Brambilla, E.; Behr, J. P. *Gene Ther.* **1996**, *3*, 1010–1017.
(26) Lin, A. J.; Slack, N. L.; Ahmad, A.; George, C. X.; Samuel, C. E.; Safinya, C. R. *Biophys. J.* **2003**, *84*, 3307–3316.
(27) Mislick, K. A.; Baldeschwieler, J. D. *Proc. Natl. Acad. Sci. U.S.A.* **1996**, *93*, 12349–12354.
(28) Zabner, J.; Fasbender, A. J.; Moninger, T.; Poellinger, K. A.; Welsh, M. J. *J. Biol. Chem.* **1995**, *270*, 18997–19007.

unit area) are trapped in endosomes,[24,26] leading to low transfection efficiency (TE; a measure of the expression of the exogenous gene that is transferred). At high σ_M (corresponding to low mole fractions of neutral lipid (Φ_{NL}) of typically less than 0.3), complexes are able to fuse with endosomal membranes, resulting in cytoplasmic delivery of complexes and higher TE.

For CL−siRNA complexes incorporating the univalent cationic lipid 1,2-dioleoyl-3-trimethylammonium-propane (DOTAP) within their membrane, however, the high σ_M regime coincided with the onset of global (nonspecific) gene silencing resulting from lipid toxicity.[29] Furthermore, incorporating the neutral lipid 1,2-dioleoyl-*sn*-glycero-3-phosphatidylethanolamine (DOPE) into these complexes (a strategy commonly and successfully employed to increase TE of CL−DNA complexes, including at low σ_M) also resulted in the onset of lipid toxicity and nonspecific gene silencing. To address this problem without having to resort to custom synthesis of multivalent lipids,[29] we applied a physicochemical approach. Using only commercially available lipids, we designed CL−siRNA complexes at low membrane charge density with membrane properties that facilitate endosomal release by promoting fusion between the membranes of the endosome and the entrapped complex.

Consideration of membrane elasticity shows that cubic phase CL−siRNA complexes should possess efficient fusogenic properties independent of membrane charge density. The elastic energy per unit area (F/A) of a lipid bilayer membrane described in the Helfrich form[30] is given by $F/A = 0.5\kappa(C - C_0)^2 + \kappa_G C_1 C_2$, where C_1 and C_2 are curvatures of the membrane, C_0 is the spontaneous curvature, and κ and κ_G are the membrane bending and Gaussian elastic moduli, respectively. The elastic moduli and C_0 are derived from the properties of the lipid molecule in its local membrane environment. The first term represents the energetic cost of bending a membrane away from C_0. For membranes with a negative Gaussian modulus, $\kappa_G < 0$, spherically shaped vesicles with positive curvature $C_1C_2 > 0$ are favored. On the other hand, membranes with a positive Gaussian modulus, $\kappa_G > 0$, will favor saddle-splay shaped surfaces with negative Gaussian curvature $C_1C_2 < 0$ such as the surfaces of bicontinuous cubic phases (cf., Figure 1) and membrane pores. Thus, cubic phase forming lipids (with $\kappa_G > 0$) should give rise to enhanced membrane fusion, which requires the spontaneous transient formation of pores with negative Gaussian curvature surfaces.[26,31] Indeed, membrane fusion mediated through the onset of pore formation has been mechanistically associated with bicontinuous cubic phase formation.[32−34]

Results and Discussion

Our study focused on the nonionic lipid glycerol monooleate (GMO, 1-monooleoyl-glycerol). The chemical structure of GMO and the other lipids used in this work is displayed in Supporting Information Figure S1. The phase diagram of GMO/water mixtures displays a large region occupied by two inverse bicontinuous cubic phases: the double gyroid phase (Q_{II}^G) for low water content (up to 30 wt %), and the double diamond phase (Q_{II}^D) for higher water contents (from 30 to 40 wt %), with crystallographic space groups *Ia*3*d* and *Pn*3*m*, respectively.[35,36] We hypothesized that CL−siRNA complexes containing GMO would form cubic phases, thereby improving endosomal escape due to enhanced fusion of complex and endosomal membrane, and thus exhibiting more efficient intracellular siRNA delivery and gene silencing.

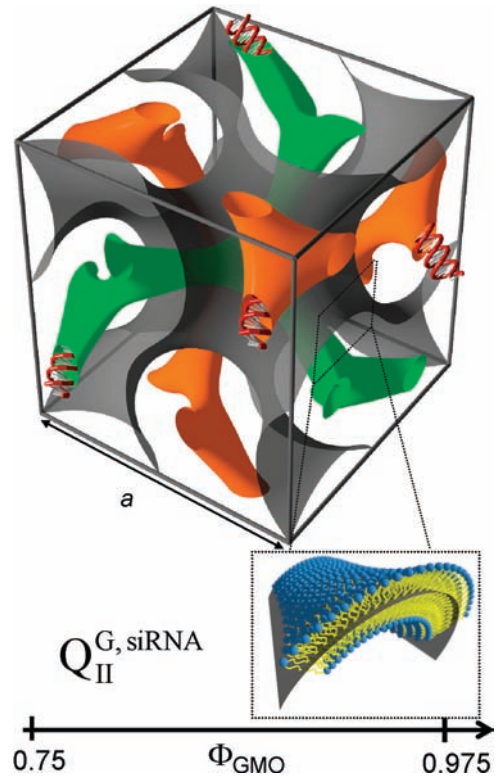

Figure 1. Illustration of a unit cell of CL−siRNA complexes in the double gyroid (*Ia*3*d*) cubic phase. The surfaces were generated in POV-Ray[42] using the level-set equations.[43] This new phase, termed $Q_{II}^{G,siRNA}$, is obtained for DOTAP/GMO−siRNA complexes for GMO molar fractions (Φ_{GMO}) of $0.75 \leq \Phi_{GMO} \leq 0.975$. A lipid bilayer surface separates two independent, continuous water channels (green and orange) containing the siRNA. For clarity, the bilayer is not shown in its entire thickness but represented by an imaginary surface (gray) corresponding to a thin layer in the center of the membrane as indicated in the enlarged inset.

Consistent with our hypothesis, we found that mixtures of GMO with DOTAP form a stable, positively charged double gyroid cubic phase ($Q_{II}^{G,LIPIDS}$). This phase allows incorporation of siRNA, leading to well-ordered CL−siRNA assemblies with a 3D bicontinuous cubic structure for molar fractions of GMO (Φ_{GMO}) of $0.75 \leq \Phi_{GMO} \leq 0.975$. Figure 1 shows a schematic representation of the unit cell of an inverse bicontinuous cubic phase ($Q_{II}^{G,siRNA}$) containing siRNA. The $Q_{II}^{G,siRNA}$ phase is comprised of a bilayer surface, that divides two intertwined but independent water channels (hosting the siRNA molecules). As anticipated, these complexes allowed for high levels of sequence-specific gene knockdown in the regime of low charge density where lamellar complexes are considerably less efficient.

Figure 2a displays synchrotron small-angle X-ray scattering (SAXS) scans of DOTAP/GMO mixtures (without siRNA) at

(29) Bouxsein, N. F.; McAllister, C. S.; Ewert, K.; Samuel, C. E.; Safinya, C. R. *Biochemistry* **2007**, *46*, 4785–4792.
(30) Helfrich, W. Z. *Z. Naturforsch.* **1973**, *C28*, 693–703.
(31) Koynova, R.; Wang, L.; MacDonald, R. C. *Proc. Natl. Acad. Sci. U.S.A.* **2006**, *103*, 14373–14378.
(32) Porte, G. *J. Phys.: Condens. Matter* **1992**, *4*, 8649–8670.
(33) Siegel, D. P.; Epand, R. M. *Biophys. J.* **1997**, *73*, 3089–3111.
(34) Yang, L.; Huang, H. W. *Science* **2002**, *297*, 1877–1879.
(35) Briggs, J.; Chung, H.; Caffrey, M. *J. Phys. II France* **1996**, *6*, 723–751.
(36) Larsson, K. *Nature* **1983**, *304*, 664–665.

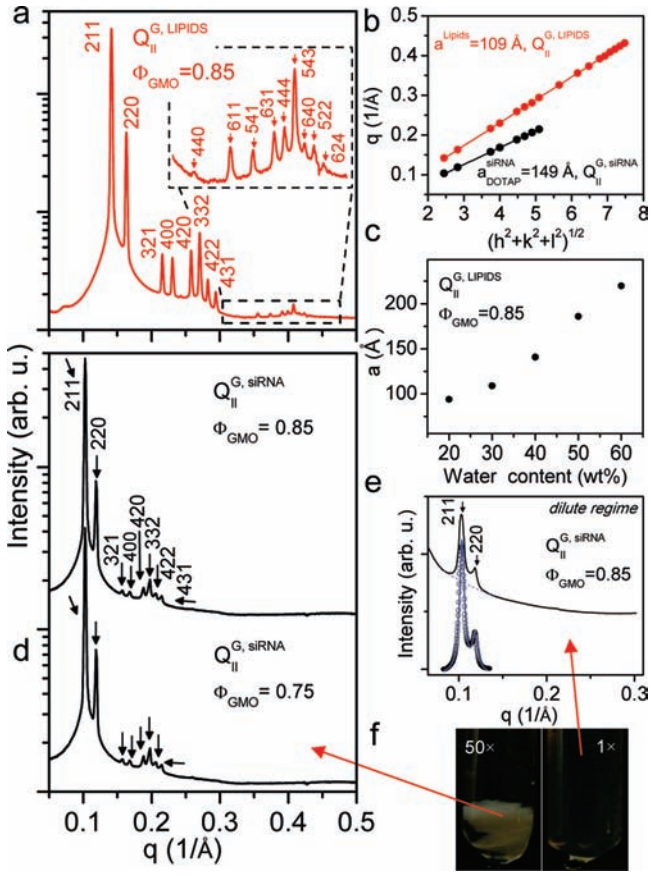

Figure 2. (a) Synchrotron small-angle X-ray scattering (SAXS) data obtained for DOTAP/GMO in 30 wt % water without siRNA at $\Phi_{GMO} = 0.85$. The large number of reflections result from a body centered gyroid cubic structure with space group *Ia*3*d*, labeled $Q_{II}^{G,LIPIDS}$ as described in the text. (b) Plot of the wave-vector q versus $(h^2 + k^2 + l^2)^{1/2}$ showing the expected straight line (with slope $2\pi/a$, where a is the unit cell dimension) for cubic phase samples (red, $Q_{II}^{G,LIPIDS}$ ($\Phi_{GMO} = 0.85$), black, $Q_{II}^{G,siRNA}$ ($\Phi_{GMO} = 0.85$)). The data points correspond to reflections shown in (a) and (d). (c) Lattice spacing of the $Q_{II}^{G,LIPIDS}$ phase as a function of water content at $\Phi_{GMO} = 0.85$. The lattice spacing increases more than 2-fold without a change in phase up to 60 wt % water. (d) SAXS data for DOTAP/GMO−siRNA complexes prepared in excess OptiMEM medium at $\Phi_{GMO} = 0.85$ (top) and at $\Phi_{GMO} = 0.75$ (bottom). The observed peaks can unambiguously be assigned to the gyroid cubic structure with space group *Ia*3*d* (termed $Q_{II}^{G,siRNA}$, cf., Figure 1) of the same nature as that obtained for DOTAP/GMO without siRNA (see text for discussion). (e) SAXS scan of a sample of DOTAP/GMO−siRNA complexes prepared at the concentration used in gene-silencing experiments (0.02 wt % in OptiMEM medium). As evident from the observed reflections, complexes retain the gyroid cubic structure ($Q_{II}^{G,siRNA}$) at this dilute concentration. The two peak positions were obtained from a fit of the X-ray profile to a double Lorentzian line shape (blue curve going through the data points shown as "○") after background subtraction of a second-order polynomial (blue dashed line). (f) Visual comparison of SAXS samples. Left: A typical sample pellet obtained by mixing concentrated lipid and siRNA solutions, as used to collect the SAXS data shown in (d). Right: A dilute uniform dispersion of lipid−siRNA complexes (0.02 wt % in water) as used to collect the SAXS data shown in (e).

a molar fraction of GMO (Φ_{GMO}) of 0.85 containing 30 wt % water. A remarkably large number of sharp peaks are observed, indicating the presence of a well-ordered 3D cubic phase. The peaks occur at the reciprocal lattice vectors $q/(2\pi/a) = G_{hkl}/(2\pi/a) = (h^2 + k^2 + l^2)^{1/2} = \sqrt{6}, \sqrt{8}, \sqrt{14}, \sqrt{16}, \sqrt{20}, \sqrt{22}, \sqrt{24}, \sqrt{26}, \sqrt{32}, \sqrt{38}, \sqrt{42}, \sqrt{46}, \sqrt{48}, \sqrt{50}, \sqrt{52}, \sqrt{54}$, and $\sqrt{56}$ corresponding to the [211], [220], [321], [400], [420], [332], [422], [431], [440], [611], [541], [631], [444], [543], [640], [552] and [721], and [624] reflections, respectively, with a representing the unit cell dimension of the cubic phase (see Supporting Information Table S1). The [521] reflection is obscured by the large tail of the [431] reflection, and a hint of the [620] reflection in the form of a bump can be seen in the high-q tail of the [611] reflection. The observed 17 X-ray reflections explicitly rule out the diamond cubic structure (space group *Pn*3*m*), while precisely satisfying the conditions required for the body centered gyroid cubic structure with space group *Ia*3*d*[37] (labeled $Q_{II}^{G,LIPIDS}$): (i) *hkl*, $h + k + l = 2n$, (ii) 0*kl*, *k*, $l = 2n$, (iii) *hhl*, $2h + l = 4n$, and (iv) *h*00, $h = 4n$ (with *h*, *k*, *l* permutable and *n* an integer).[37−39] As expected for a cubic phase, a plot of the X-ray wave-vector q versus $(h^2 + k^2 + l^2)^{1/2}$ for the observed Bragg reflections exactly fits a straight line with slope $2\pi/a$ (Figure 2b, the data points correspond to all observed reflections). The lattice spacing for the cubic phase of DOTAP/GMO without siRNA for $\Phi_{GMO} = 0.85$ at 30 wt % water is $a^{Lipids} = 109$ Å. This is close to what is obtained for the gyroid *Ia*3*d* phase of pure GMO at 30 wt % water.[36] The cationic cubic structure is able to swell up to 60 wt % of water without a phase transition, with lattice dimensions covering a range from below 100 to over 200 Å (cf., Figure 2c). In contrast, the neutral GMO/water system undergoes a phase transition at 35 wt % of water, from the *Ia*3*d* phase to the diamond-type cubic phase with space group *Pn*3*m*. A similar shift in the phase boundaries has been observed for negatively charged cubic phases prepared by the addition of anionic lipids to the GMO/water system.[38]

The ability of the cationic cubic DOTAP/GMO phase to swell greatly while retaining the *Ia*3*d* cubic structure likely facilitates incorporation of siRNA and thus formation of stable cubic phase CL−siRNA complexes. Figure 2d displays SAXS scans of isoelectric ($\rho = 1$) DOTAP/GMO−siRNA complexes at $\Phi_{GMO} = 0.75$ and $\Phi_{GMO} = 0.85$ (black lines) in excess OptiMEM medium. These complexes are stoichiometrically neutral, with the negative phosphates on the siRNA backbone balanced by the positive charges of the lipids: $\rho = N(+)/N(-) = n_{CL}/n_{siRNAb} = 1$, where n_{CL} and n_{siRNAb} are the amounts (in mol) of cationic lipid and siRNA bases, respectively. The eight reflections observed in the X-ray profile correspond to the first eight reflections observed for the $Q_{II}^{G,LIPIDS}$ phase, with the plot of q versus $(h^2 + k^2 + l^2)^{1/2}$ again fitting a straight line (Figure 2b, black line/dots, $\Phi_{GMO} = 0.85$). This new phase of CL−siRNA complexes (labeled $Q_{II}^{G,siRNA}$ (cf., Figure 1)) can thus be unambiguously assigned to the gyroid cubic structure with space group *Ia*3*d* as obtained for DOTAP/GMO without siRNA. The lattice spacing of the $Q_{II}^{G,siRNA}$ phase, $a^{siRNA} = 149$ Å, is equivalent to that of a DOTAP/GMO/water cubic phase containing about 40 wt % water. The observation of a larger number of reflections for the cubic phase without siRNA as compared to CL−siRNA complexes is not unexpected. In the absence of siRNA, the charged DOTAP/GMO membranes forming the pores of the cubic phase resist large thermal fluctuations due to long-range electrostatic repulsions. The addition of oppositely charged siRNA in CL−siRNA complexes effectively screens the electrostatic interactions, which in turn allows for larger membrane thermal fluctuations that rapidly suppress higher-order reflections because of the X-ray Debye−Waller

(37) Hahn, T. *International Tables for Crystallography*, 3rd ed.; Kluwer Academic: Dordrecht/Boston/London, 1992; Vol. A, Space-group symmetry.
(38) Engblom, J.; Miezis, Y.; Nylander, T.; Razumas, V.; Larsson, K. *Prog. Colloid Polym. Sci.* **2000**, *116*, 9–15.
(39) Roux, D.; Safinya, C. R. *J. Phys. (Paris)* **1988**, *49*, 307–318.

factor.[39] As an important aside, we found that the cubic phase could not be stabilized with long DNA molecules for any lipid composition regime (see Supporting Information Figure S2).

Importantly, we found that the internal structure of cubic DOTAP/GMO−siRNA complexes remained unchanged when samples were prepared as for the gene silencing experiments described below, that is, at much lower concentration than typically used for SAXS experiments. Figure 2e displays a SAXS profile for such a dilute sample (containing only 0.02 wt % of DOTAP/GMO−siRNA complexes in OptiMEM medium). Two strong reflections are readily observed (q = 0.1032 and 0.1189 Å^{-1}) at the same position as in the corresponding concentrated sample. These are consistent with the two first reflections ([211] and [220]) of the gyroid cubic phase with a lattice cubic dimension of a = 149 Å (see Supporting Information Table S1).

The relative peak positions, that is, the ratio of the observed wave vectors q for the dilute sample, are consistent exclusively with a gyroid phase. For the gyroid phase, the expected ratio is $q_{221}/q_{220} = \sqrt{6}/\sqrt{8} = 0.866$. The experimentally obtained ratio is $q_{221}/q_{220} = 0.1032/0.1189 = 0.868$. It could be argued that phase coexistence would give rise to a set of peaks in the same q-range. However, the ratios expected for coexistence of the lamellar (q_{001} = 0.1072 1/Å) and the inverse hexagonal (q_{01} = 0.1215 1/Å) phases and for coexistence of the cubic and the inverse hexagonal phases are 0.882 and 0.850, respectively. Both values are significantly different from the observed ratio. In addition, for the case of phase coexistence, the lipid composition of the dilute complexes would have to be different than the nominal composition of $\Phi_{GMO} = 0.85$ (where the gyroid phase is found at higher concentrations). Fluorescence microscopy of dilute complexes (Figure 3; discussed in detail below) rules out this possibility by showing no evidence of coexistence of complexes with lipid-only aggregates (which would be clearly observable in the lipid fluorescence mode).

The two peak positions were determined quantitatively by a nonlinear least-squares fit of the X-ray profile to a double Lorentzian line shape (solid blue line going through the data shown as "○" in Figure 2e) after a second-order polynomial background reduction (dashed blue line in Figure 2e). In the dilute sample, only two reflections are observed due to the lower concentration and the broadened peaks. The concentrated samples have been centrifuged into a dense pellet, allowing the complex membranes to fuse and efficiently giving rise to large domains and sharp X-ray peaks. In contrast, the dilute sample has not undergone centrifugation and consists of small clusters of complex particles (as seen in the DIC images of Figure 3). The domain sizes are therefore much smaller in the dilute sample, giving rise to the broader peaks in the X-ray profile. Figure 2f shows a visual comparison of this sample and a typical sample used for the SAXS measurements shown in Figure 2d, which were prepared at 1.1 wt % of DOTAP/GMO−siRNA in OptiMEM medium. While the latter contains a distinct pellet (Figure 2f, left), the former appears as a dilute, uniform solution of complexes with no pellet (Figure 2f, right).

The morphology of the DOTAP/GMO−siRNA lipid complexes in the cubic phase regime was investigated using differential-interference-contrast (DIC; Figure 3, left panel) and fluorescence optical microscopy (Figure 3, middle and right panels). Stoichiometrically neutral complexes (ρ = 1) consist of aggregates of connected globules, which became significantly smaller for negatively charged (ρ = 0.5) or positively charged (ρ = 2) complexes, most likely due to electrostatic repulsion.

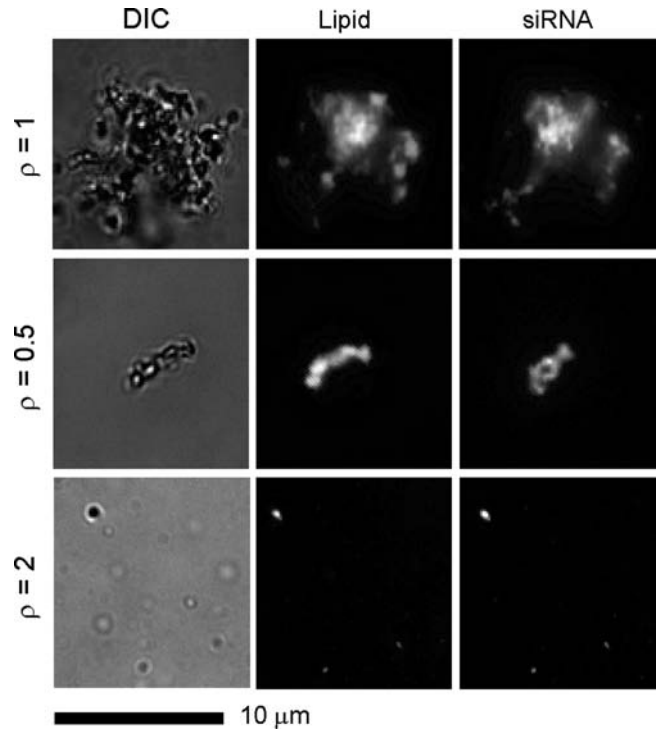

Figure 3. Optical microscopy images of DOTAP/GMO−siRNA complexes in the cubic phase region (Φ_{GMO} = 0.85) at different lipid to siRNA charge ratios, ρ. Complexes were viewed in differential-interference-contrast (DIC) (left), lipid fluorescence (middle), and siRNA fluorescence mode (right). As evident from these images, lipids and siRNA are completely colocalized. The observed aggregates are smaller for complexes prepared with excess siRNA (ρ = 0.5) or excess cationic lipid (ρ = 2) than for stoichiometrically neutral complexes (ρ = 1).

The observed overlay of lipid and siRNA distributions in the two fluorescence modes (Figure 3, middle and right panels) indicates that the complexes consist of colocalized lipid and siRNA domains. Further confirmation that the siRNA is indeed incorporated in the bicontinuous lipid phase is provided by the efficient silencing mediated by the complexes (see below) as well-spectrophotometric measurements of siRNA concentration (below 5% of total siRNA for ρ = 1 and ρ = 2) in the supernatant of samples prepared for SAXS experiments (data not shown).

The phase behavior of DOTAP/GMO−siRNA complexes is rich: as Φ_{GMO} is decreased below 0.75, two other previously observed CL−siRNA complex phases are found. These include a 2D hexagonal array of lipid tubules (inverse cylindrical micelles) decorating siRNA (H_{II}^{siRNA}) and eventually ($0.60 \geq \Phi_{GMO} \geq 0$) a stack of lipid bilayers with an intercalated layer of siRNA molecules in a 2D isotropic phase (L_{α}^{siRNA}), with a coexistence region for Φ_{GMO} = 0.65. Figure 4a schematically depicts these phases. As shown in Figure 4b, the lamellar phase (for Φ_{GMO} = 0.50) is characterized by sharp peaks at q_{001} = 0.109 Å^{-1} and q_{002} = 0.218 Å^{-1}, resulting from the layered structure with periodicity $d = 2\pi/q_{001} = 57.14$ Å. A broad peak, resulting from weak correlations between the short siRNA molecules,[29] is evident between q_{001} and q_{002}. The H_{II}^{siRNA} phase at Φ_{GMO} = 0.70 is characterized by the appearance of four Bragg peaks (q_{10}, q_{11}, q_{20}, and q_{21} with $q_{hk}/q_{10} = 1{:}\sqrt{3}{:}\sqrt{4}{:}\sqrt{7}$), corresponding to a hexagonal lattice spacing of $a_H = 4\pi/[\sqrt{3}q_{10}]$ = 52.8 Å (q_{10} = 0.119 Å^{-1}). The lattice spacings obtained from the SAXS data for lipid−siRNA complexes in the three phases are displayed in Supporting Information Figure S3.

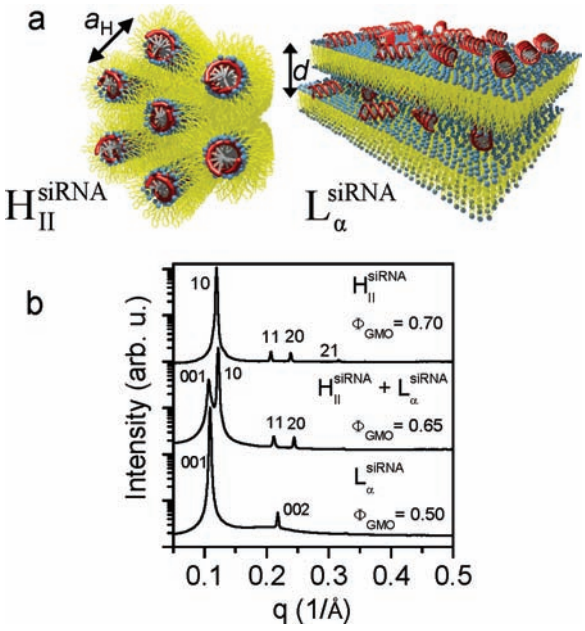

Figure 4. DOTAP/GMO−siRNA complexes exhibit a rich phase behavior, forming the previously observed lamellar and inverted hexagonal structures (at low molar fraction of GMO (Φ_{GMO})) in addition to the bicontinuous cubic phase. (a) Schematic depiction of the inverted hexagonal (H_{II}^{siRNA}) and the lamellar (L_α^{siRNA}) phases of CL−siRNA complexes. (b) Typical SAXS profiles of DOTAP/GMO−siRNA complexes for $\Phi_{GMO} \leq 0.70$. The characteristic scattering patterns of the H_{II}^{siRNA} and the L_α^{siRNA} phase (see text) are observed at $\Phi_{GMO} = 0.70$ and $\Phi_{GMO} = 0.50$, respectively. Reflections from both structures are observed at $\Phi_{GMO} = 0.65$, indicating coexistence of the two phases.

We performed gene-silencing experiments to investigate the gene knockdown activity of the new cubic phase as a carrier of exogenous siRNA. The silencing efficiency (SE; a measure of post-transcriptional, specific silencing of the gene targeted by the transferred siRNA) of the complexes was studied at different charge ratios (ρ) and neutral lipid contents (Φ_{NL}) and compared to that of lamellar complexes. We used a dual luciferase assay, which allows simultaneous measurement of total as well as nonspecific silencing.[29] Mouse L-cells were simultaneously transfected with two distinct plasmids, one encoding the firefly (FF) luciferase and the other the Renilla (RL) luciferase gene. The cells were then treated with CL−siRNA complexes comprising siRNA targeting the FF luciferase mRNA for sequence-specific degradation. A dual luciferase assay was used to measure the expression of the targeted FF and the nontargeted RL luciferases, yielding the bioluminescence of the respective luciferases (labeled $FF_{CL-siRNA\ treated}(\Phi_{NL},\rho)$ for firefly and $RL_{CL-siRNA\ treated}(\Phi_{NL},\rho)$ for Renilla). Simultaneous control experiments on a similar number of cells that were not treated with CL−siRNA complexes yielded $FF_{untreated}$ and $RL_{untreated}$. The total gene knockdown determined as $K_T = 1 - FF_{CL-siRNA\ treated}(\Phi_{NL},\rho)/FF_{untreated}$ represents the sequence-specific silencing of the target FF luciferase by the delivered siRNA together with any nonspecific silencing. The nonspecific gene knockdown is determined as $K_{NS} = 1 - RL_{CL-siRNA\ treated}(\Phi_{NL},\rho)/RL_{untreated}$, which measures the global inhibition of protein synthesis due to off-target silencing and toxicity of CL−siRNA complexes. Optimal gene silencing would correspond to K_T approaching unity and K_{NS} approaching zero.[29]

Figure 5a shows the total and nonspecific knockdown, K_T and K_{NS}, as a function of mole fraction of neutral lipid, Φ_{NL}, at fixed $\rho = 5$ for CL−siRNA complexes using GMO (□) or 1,2-dioleoyl-*sn*-glycero-3-phosphocholine (DOPC) (○) as neutral lipids and DOTAP as the cationic lipid. The three composition regions corresponding to the cubic ($Q_{II}^{G,siRNA}$), the inverted hexagonal (H_{II}^{siRNA}), and the lamellar (L_α^{siRNA}) phases of DOTAP/GMO−siRNA complexes are indicated. The DOPC-containing complexes retain the lamellar L_α^{siRNA} phase throughout the entire lipid composition region.[29] For $\Phi_{NL} < 0.65$ (in the lamellar phase), the total gene knockdown, K_T, remains essentially constant (reaching between ~0.75 and 0.70) for GMO-containing complexes and is systematically lower (between ~0.5 and 0.45) for DOPC-containing complexes. The most dramatic difference is observed at high contents of neutral lipid, where the gyroid cubic phase obtained with GMO is far superior than the lamellar phase obtained using DOPC. The nonspecific gene knockdown remains near zero for $\Phi_{NL} > 0.4$ for both systems and then starts to increase significantly to values of $K_{NS} \approx 0.2$. Interestingly, GMO-containing complexes in the H_{II}^{siRNA} phase also exhibit high total and low nonspecific silencing. This is in contrast to what was previously observed for inverted hexagonal phases comprising DOPE,[29] suggesting that DOPE rather than the inverse hexagonal phase causes nonspecific silencing (due to cytotoxicity).

Figure 5b plots the total and nonspecific knockdown, K_T and K_{NS}, for complexes with the same components as in Figure 5a, but now as a function of the charge ratio ρ at fixed siRNA concentration and $\Phi_{NL} = 0.85$. At this Φ_{NL}, the GMO-containing complexes are in the cubic phase, and the DOPC-containing complexes are in the lamellar phase. Over the entire range of ρ, complexes in the cubic $Q_{II}^{G,siRNA}$ phase (□) exhibit remarkably higher total gene knockdown than complexes in the L_α^{siRNA} phase (○). Nonspecific silencing, as measured by K_{NS}, remains reasonably low ($0 \leq K_{NS} \leq 0.2$) for both systems up to $\rho = 10$.

At $\Phi_{NL} = 0.85$, the charge density (σ_M) of the lipid bilayer is very low, and the low silencing efficiency of the L_α^{siRNA} phase may be attributed to endosomal entrapment, as previously demonstrated for DNA complexes at low σ_M (where the weak electrostatic attraction between the complex and the endosomal membrane fails to promote fusion events leading to cytoplasmic delivery).[24,26] On the other hand, the cubic ($Q_{II}^{G,siRNA}$) CL−siRNA complexes are able to escape from endosomes, as their high SE unequivocally demonstrates. This indicates that the mechanism of endosomal escape involves more than electrostatic interactions. As described earlier, lipids forming inverse bicontinuous cubic phases have a positive Gaussian modulus ($\kappa_G > 0$), which tends to drive the spontaneous formation of negative Gaussian curvature interfaces, such as membrane pores. Thus, we attribute the significantly higher silencing efficiency to the ability of the cubic phase to mediate enhanced fusion between the membranes of the complex and the endosome.

Because lipid-based carriers of siRNA are often plagued by undesired toxicity, we employed a tetrazolium salt-based assay[40] to monitor cell viability in the presence of various cubic and lamellar CL−siRNA complexes. Figure 5c compares the percentage of viable cells for DOTAP/GMO−siRNA complexes in the cubic phase and DOTAP/DOPC−siRNA complexes in the lamellar phase (as a reference) as a function of total lipid concentration. Because siRNA concentration and total sample volume are kept constant, the charge ratio ρ is also a measurement of the lipid concentration and is represented on the top

(40) Cory, A. H.; Owen, T. C.; Barltrop, J. A.; Cory, J. G. *Cancer Commun.* **1991**, *3*, 207–212.

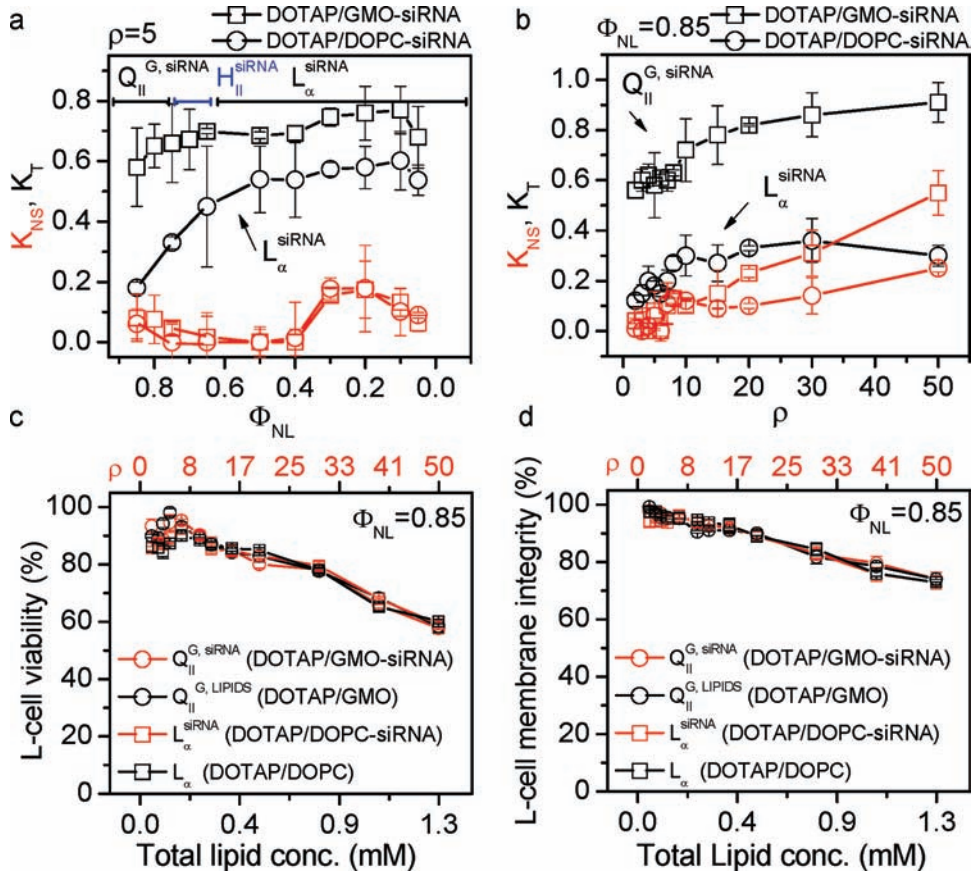

Figure 5. Total (K_T, black lines and symbols) and nonspecific (K_{NS}, red lines and symbols) gene knockdown for DOTAP/GMO−siRNA complexes (□) and DOTAP/DOPC−siRNA complexes (○) (a) as a function of mole fraction of neutral lipid (Φ_{NL}) at fixed $\rho = 5$, and (b) as a function of ρ at fixed $\Phi_{NL} = 0.85$. Complexes in the cubic phase ($Q_{II}^{G,siRNA}$) at low cationic lipid content ($\Phi_{GMO} \geq 0.75$) show remarkably improved specific silencing over complexes in the lamellar phase (L_{α}^{siRNA}). (c) Cell viability and (d) membrane integrity as a function of total lipid concentration for cells incubated with $Q_{II}^{G,siRNA}$ DOTAP/GMO−siRNA complexes and L_{α}^{siRNA} DOTAP/DOPC−siRNA complexes (red ○ and □, respectively), and with the corresponding DOTAP/GMO and DOTAP/DOPC lipid mixtures without siRNA (red and black ○ and □, respectively). The top *x*-axis indicates the corresponding charge ratio, ρ, for samples containing siRNA. Both cell viability and membrane integrity remain around 90% up to remarkably high lipid concentrations and values of ρ. Notably, both measures of cytotoxicity are unaffected by the phase of the complexes as well as the presence or absence of siRNA.

x-axis. There is no observable difference between the two lipid systems, showing that GMO-based complexes are no more toxic than their DOPC-based counterparts. Moreover, cell viability is the same whether or not siRNA is present, indicating that the lipid component is responsible for cytotoxicity. The cell viability is steady at about 90% for lipid concentrations up to 0.25 mM, which corresponds to $\rho = 10$ for CL−siRNA lipid complexes. Beyond this value, viability monotonically decreases, which correlates with the onset of nonspecific silencing events (cf., Figure 5b) and suggests that the off-target inhibition of protein production is triggered by (lipid) toxicity. The cytotoxicity measurements confirm that the cubic phase (existing exclusively at high GMO contents) can be used for highly efficient gene silencing without compromising cell proliferation. Because we designed the cubic phase CL−siRNA complexes to facilitate the formation of transient pores in endosomal membranes, we also wanted to assess cytotoxicity with an assay that addresses plasma membrane integrity. Thus, we used a standard assay measuring extracellular levels of lactate dehydrogenase to quantify the amount of cells with compromised plasma membranes. The obtained results are shown in Figure 5d. The membranes of the cells remain essentially intact up to a lipid concentration of 0.4 mM, corresponding to a charge ratio $\rho = 17$ for both the GMO-containing $Q_{II}^{G,siRNA}$ complexes and the DOPC-containing L_{α}^{siRNA} complexes. The cubic phase apparently does not compromise the plasma membrane despite its intrinsic ability to promote pore formation (highlighted by the silencing results). Likely, this is because the plasma membrane is protected by its glycocalix. In addition, the confinement of the nanostructured cubic complex within the endosomal compartment allows for a large number of intermembrane collisions (leading to fusion events) as compared to the few collisions between the complex and the plasma membrane before endocytosis.

Conclusions

In addition to its widespread applications in functional genomics, siRNA technology promises to revolutionize biotechnology and therapeutics. However, the current limiting step in realizing the full potential of siRNA-based gene silencing technology is the development of efficient chemical carriers of siRNA with low toxicity. Cationic lipids constitute the key component of the vast majority of synthetic carriers (including commercially available reagents) of siRNA for gene silencing. We have presented the development of a highly efficient lipid carrier of siRNA based on a rational design of the physicochemical properties of the carrier membrane, enabling improved endosomal escape and cytoplasmic delivery of lipid−siRNA complexes. To our knowledge, this is the first time that a bicontinuous cubic phase incorporating short double-stranded

siRNA molecules within its water channels has been unambiguously demonstrated. This was achieved by using two commercially available components: a classic cubic phase-forming neutral lipid (GMO) in combination with the univalent cationic lipid DOTAP. The positively charged cubic matrix is an excellent host for short siRNA molecules due to its high ability to greatly swell while retaining the *Ia3d* space group. Significantly, this new vector is remarkably efficient in delivering siRNA for sequence-specific mRNA degradation in a regime of low membrane charge density. Most other complexes in this regime remain trapped within endosomes because weak electrostatic attractions between the membranes of complexes and endosomes fail to promote fusion and endosomal escape. The high degree of silencing is achieved with virtually no negative implications for cell viability and plasma membrane integrity, which we attribute to the low charge density of the cubic phase membranes. The mechanism suggested to explain the efficiency of the cubic phase relates to the intrinsic property of bicontinuous phases (with membranes with positive Gaussian modulus) to spontaneously drive the formation of dynamical transient pores that promote fusion between the outer membrane of CL−siRNA complexes and the adjacent endosomal membrane.

Experimental Section

The methods used have been described in detail elsewhere.[29,41] Here, we provide a brief description.

Liposome Preparation. DOTAP and DOPC were purchased from Avanti Polar Lipids. GMO was obtained from Nu-Check-Prep. All lipids were used as received. Liposomes were prepared by dissolving the lipid powders in chloroform, combining the solutions at the desired volumetric ratios and then evaporating the solvent, first under a stream of nitrogen and then in a vacuum overnight. The resulting lipid film was hydrated at 37 °C for 2 h with sterile water (18.2 MΩ cm) from a Milli-Q filtration system (Millipore). The final lipid concentration was 40 mM (for SAXS) and 1 mM (for SAXS of dilute samples and cell culture studies). All solutions were tip-sonicated (Vibra-cell, Sonics Materials) and stored at 4 °C.

X-ray Samples. CL−siRNA complexes were prepared in quartz capillaries (Hilgenberg Glas, Germany) by mixing liposome solution with 50 μg of siRNA (19 base pair: CUUACGCUGAGUACUUCGA with two 3′-deoxythymidine overhangs, from Dharmacon, at 10 μg/μL). This siRNA sequence was chosen to specifically target the firefly luciferase gene.[29] The samples were mixed for 15 min at 4 °C using a table-top centrifuge and flame-sealed before storage at 4 °C. Synchrotron SAXS experiments were conducted at the Stanford Synchrotron Radiation Lightsource, beamline 4-2. The 2D powder diffraction data were radially averaged upon acquisition on a MX-225 CCD detector (Rayonics) and integrated using SAXSi (MATLAB based GUI, authored by Roy Beck). The X-ray data for the dilute sample were fit to a double Lorentzian line shape after background subtraction (of a second-order polynomial function). For lipid-only samples, lipid films (from 40 mM chloroform solutions) were prepared in glass ampules and hydrated at 40 °C overnight with the desired amount of water. The resulting mixtures were centrifuged at 5000 rpm for 30 min, flame-sealed, then turned end over end and centrifuged again until mixing was complete.

Optical Microscopy. For fluorescence microscopy experiments, siRNA was labeled with YoYo-1 iodide (Molecular Probes) using one dye molecule per 15 bp, and 0.2 mol % of the lipid dye DHPE-Texas Red (Molecular Probes) was added to the liposomes. The CL−siRNA complexes at $\rho = 0.5$, 1, and 2 were prepared from solutions containing 0.01 mg/mL siRNA and 0.1 mg/mL lipids.

Gene Silencing. Mouse fibroblast L-cells were seeded into 24-well plates at 85 000 cells per well 24 h before they were transfected with luciferase DNA plasmids (pGL3 firefly and phRL Renilla; both from Promega) using Lipofectamine 2000 (L2000, Invitrogen) as transfecting agent. A ratio of 380 ng of pGL3 to 20 ng of phRL to 1 μL of L2000 per 200 μL of OptiMEM (Invitrogen) was used to form the complexes added to each well. After a transfection period of 6 h, the cells were washed, and CL−siRNA complexes containing 0.266 μg siRNA targeting the firefly luciferase (same siRNA as for SAXS experiments) were added. The amount of cationic lipid was determined by $\rho = N_{(+)}/N(-) = n_{CL}/n_{siRNAb}$, and lipid composition by the mole fraction NL (Φ_{NL}) present in the liposomes. CL−siRNA complexes were mixed for 30 min prior to their addition to the cells and were allowed to incubate on the cells for 3 h before maintenance medium was added. Cells were harvested 20 h later in 150 μL of passive lysis buffer (Promega). Sixteen microliters of lysate extract was used in the Dual Luciferase Assay (Promega). A multilabel counter (1420 Victor3 V, Perkin-Elmer) was used to measure bioluminescence in relative light units (RLU).

Cytotoxicity. Cytoxicity was assessed using the CellTiter 96 aqueous assay (Promega) for cell viability and the CytoTOX ONE assay (Promega) for membrane integrity. Mouse fibroblast L-cells were seeded in 96-well plates 18 h prior to treatment. The number of cells and amount of CL−siRNA complexes were scaled down by a factor of 5 over what was used in experiments using 24-well plates. Cells were incubated with complexes or corresponding liposomes for 3 h. As controls, some wells were left untreated (no complexes or liposomes) to allow for normalization. After incubation, the recommended volumes of assay were added to each well, and cell viability/cytotoxicity was measured as per the assay manufacturer's instructions.

Acknowledgment. We acknowledge discussions on the cubic structure with Ram Seshadri. Funding was provided by NIH GM-59288 (structure-biological activity studies), DOE-BES grant number DOE-DE-FG02-06ER46314 (liposome−nucleic acid cubic phase structure), and NSF DMR-0803103 (phase behavior). C.L. was funded by the Swedish Research Council (VR) and in part by DOE-BES. The X-ray diffraction work was carried out at the Stanford Synchrotron Radiation Lightsource (SSRL) beamline 4.2.

Supporting Information Available: Lipid molecular structures, SAXS data obtained for lipid−DNA complexes, lattice spacings for the lipid−siRNA phases, table of detailed SAXS results for the data presented in Figure 2, and complete citation details of ref 9. This material is available free of charge via the Internet at http://pubs.acs.org.

JA1059763

(41) Rädler, J. O.; Koltover, I.; Salditt, T.; Safinya, C. R. *Science* **1997**, *275*, 810–814.
(42) POV-Ray (www.povray.org).
(43) Wohlgemuth, M.; Yufa, N.; Hoffman, J.; Thomas, E. L. *Macromolecules* **2001**, *34*, 6083–6089.